PCCP

COMMUNICATION

View Article Online
View Journal | View Issue

Cite this: *Phys. Chem. Chem. Phys.*, 2023, **25**, 5343

Received 27th September 2022,
Accepted 24th January 2023

DOI: 10.1039/d2cp04516h

rsc.li/pccp

Electron-decoupled MAS DNP with N@C_{60}

Nicholas Alaniva,* [ab] Edward P. Saliba,† [bc] Patrick T. Judge,† [b] Erika L. Sesti,† [b] Wolfgang Harneit, [d] Björn Corzilius [e] and Alexander B. Barnes [a]

Frequency-chirped microwaves decouple electron- and ^{13}C-spins in magic-angle spinning N@C_{60}:C_{60} powder, improving DNP-enhanced ^{13}C NMR signal intensity by 12% for 7 s polarization, and 5% for 30 s polarization. This electron decoupling demonstration is a step toward utilizing N@C_{60} as a controllable electron-spin source for magic-angle spinning magnetic resonance experiments.

Electron decoupling improves nuclear magnetic resonance (NMR) signal that has been enhanced by dynamic nuclear polarization (DNP).[1,2] Techniques for DNP enhancement often utilize doped radical electrons as a source of relatively high polarization and microwave irradiation to facilitate transfer of polarization to nuclear spins in dipolar contact with the electron spins, with spin diffusion sending the polarization to nuclear spins not coupled to the electron spin.[3–5] Following polarization transfer, this dipolar contact reduces NMR signal intensity and resolution. The improvement afforded by electron decoupling comes from the attenuation of the electron-nuclear dipolar contact, by way of on-resonance, frequency-chirped microwave pulses. Combined with advances in cryogenic magic-angle spinning (MAS) NMR instrumentation, electron decoupling has been an effective tool for in-cell DNP NMR spectroscopy and a necessary component for "direct DNP" and MAS electron spin relaxation experiments.[6–8] To date, these experiments have employed only trityl, (Finland radical) and trityl derivatives as a polarizing agent.[9,10] Here, the utility of electron decoupling is expanded to the electron spin-3/2 of a nitrogen atom trapped in C_{60} fullerene (hereon referred to as N@C_{60}, and represented in Fig. 1, in a corner call-out).[11–14] Decoupling the electron spin in N@C_{60} improves ^{13}C signal intensity by 5% and 12% following a DNP-transfer period of 30 and 7 seconds, respectively, at 4.0 kHz MAS and 90 K.

The symmetry of the C_{60} cage (*g*-tensor value = 2.0024) and a sparse spin-interaction network in 160 parts-per-million (ppm) N@C_{60} : C_{60} ($160:10^6$) poly-crystalline powder result in one of the narrowest electron paramagnetic relaxation (EPR) signals in solid state (Fig. 1).[15,16] The spin-spin relaxation of the N@C_{60} electron spin is tens of microseconds (inhomogeneous contribution in this sample due to crystalline imperfections), up to an order of magnitude greater than that of other narrow-line radicals, such as trityl and BDPA, used for DNP.[17–20] Additionally, the symmetric environment, even below the polycrystalline phase transition temperature, and the near absence of *g*-anisotropy give rise to a zero-field splitting of 0.52 MHz.[16] Even considering the proportionally greater dipolar coupling due to the electron spin quantum number of 3/2, the stability

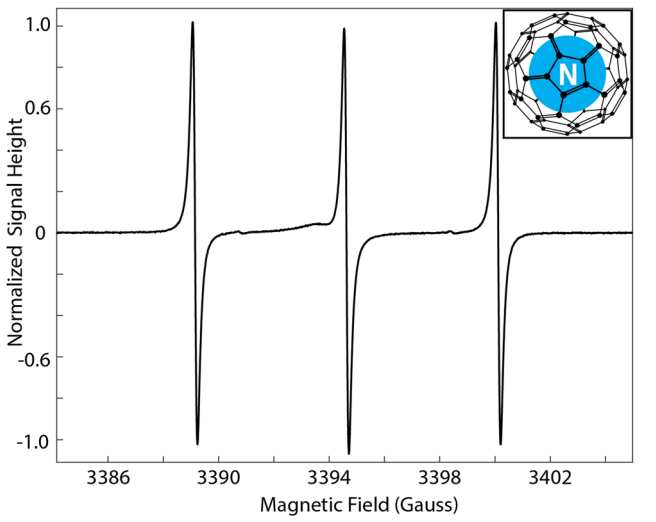

Fig. 1 EPR spectrum of 160 ppm N@C_{60}, experiment performed on Bruker X-band (10 GHz) spectrometer at 298 K. 5.68 Gauss splitting corresponds to a 15.9 MHz hyperfine-dipolar coupling. Featured in the outlined callout is a representation of an N@C_{60} molecule.

[a] *Laboratory of Physical Chemistry, ETH Zürich, Zürich 8093, Switzerland. E-mail: nalaniva@ethz.ch; Tel: +41 44 633 43 81*
[b] *Washington University in St. Louis, St. Louis 63130, MO, USA*
[c] *Massachusetts Institute of Technology, Cambridge 02139, MA, USA*
[d] *Department of Physics, Universität Osnabrück, Osnabrück 49076, Germany*
[e] *Institute of Chemistry, Department Life, Light & Matter, Universität Rostock, 18059 Rostock, Germany*
† These authors contributed equally to this work.

and electron relaxation of N@C_{60} make it a sensible target for electron decoupling, and DNP experiments with electron spin control.

While higher-power microwave devices are being developed for MAS DNP application (gyrotrons, gyro-amplifiers), current frequency-agile gyrotrons are able to produce shaped microwave pulses (chirps, sweeps) that cover the frequency range of the targeted electron spin resonance and exert control over the spin.[21–23] A narrow electron spin resonance reduces the required frequency range of this chirped pulse to control the spin. The EPR signal from N@C_{60} is so narrow that electron spin control with hard pulses will be possible with existing frequency-agile gyrotron technology.[24] The gyrotron used for these experiments generates an approximate microwave Rabi frequency of 0.38 MHz at the sample, which is on the order of the electron-^{13}C (local ^{13}C, on the N@C_{60} cage, itself) hyperfine dipolar coupling (predicted at 0.44 MHz; 1.3 MHz for $\pm 3/2$ spin - measured to be 0.30 MHz, however).[16,25] Although certain pulsed-DNP mechanisms require currently-inaccessible microwave Rabi frequencies (at high magnetic field), there are some that become possible with such a ''narrow-line'' radical.[2,26–29] Demonstration of electron decoupling on this 160 ppm N@C_{60}:C_{60} poly-crystalline powder is the first step toward pulsed DNP MAS and pulsed EPR MAS using the N@C_{60} electron spin.

The experiments here are performed on a relatively dilute collection of electron spins. For effective use of N@C_{60} as a polarizing agent, 100% pure N@C_{60} will be required. The dipolar linewidth at 100% approximates 60 Gauss, but when diluted to lower concentration in a sample of interest, this interaction will be reduced and the corresponding linewidths narrow.[30] Current limitations regarding the methods of endofullerene generation (ion implementation, gas-discharge, and radio-frequency plasma discharge) and purification, using high-performance liquid chromatography, severely restrict access to milligram-amounts of pure N@C_{60}.[31–37] Dissemination of endofullerene production and optimization of formation methods is a path toward production of realistic amounts of pure N@C_{60} for experiments. However, currently-accessible quantities of pure N@C_{60} would be sufficient for DNP NMR MAS experiments that utilize small sample volumes (1 μL and lower), which have been demonstrated using 2 mm MAS spherical rotors. However accomplished, the protection and symmetry afforded the electron spin by the C_{60} cage, the affinity of C_{60} for plasma membrane incorporation, and the capability of C_{60}-functionalization make a variety of endofullerenes promising agents for powerful magnetic resonance experiments in burgeoning areas of science, such as in-cell DNP/EPR, inorganic/surface-DNP/EPR, and quantum computing.[38,39]

The electron-decoupled MAS DNP experiments presented here use a cryogenic-MAS radio-frequency probe for excitation and detection of nuclear spins, and a frequency-agile gyrotron for control of electron spins and transfer of polarization (DNP).[22,40] Fig. 2 shows the pulse sequences used to probe the electron decoupling effect. On the ''electron channel'' line, there are 3 different conditions: DNP, electron decoupling, and

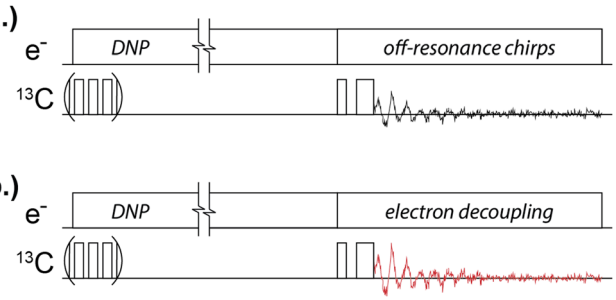

Fig. 2 ^{13}C-Hahn echo pulse sequences for DNP experiments without (a) and with (b) electron decoupling. The break in the DNP segment indicates its length in time is orders of magnitude greater than that of the other events in the sequence.

off-resonance chirps. The microwave power for each event is constant, and each event is characterized by different microwave frequency/frequencies. During DNP, the transfer of electron polarization to ^{13}C spins is facilitated by microwave irradiation at 197.484 GHz. This satisfies the double-quantum solid effect condition ($\nu_{e,Larmor} - \nu_{^{13}C,Larmor}$). The solid effect is the ''active'' DNP mechanism since the inhomogeneous linewidth of the N@C_{60} electron resonance is less than the nuclear Larmor frequency. During electron decoupling (Fig. 2b), the microwave frequency is time-dependent, changing according to a chirped triangle-waveform that covers a 60 MHz range, centered over the electron resonance frequency (197.559 GHz), in 6.63 μs.[1] This range is large enough to ensure that the chirp covers the entirety of the N@C_{60} electron spin resonance. The off-resonance chirps shown in the Fig. 2a sequence describe a frequency-chirped waveform of the same magnitude and shape, but is centered at 197.409 GHz (75 MHz below the DNP condition) so that electron spins remain unaffected. This control experiment provides a DNP-enhanced NMR signal to which the electron-decoupled signal is compared.

The exact microwave frequencies required to meet these conditions are verified experimentally with the construction of a ''DNP profile'' (Fig. 3). Each point on the profile indicates the intensity of ^{13}C NMR-signal with microwave irradiation of the frequency corresponding to its place along the horizontal axis. The spacing between the enhancement local maxima correspond to the 15.9 MHz hyperfine splitting, as observed in the N@C_{60} EPR spectrum (Fig. 1). The difference in resolution between the EPR spectrum and the DNP profile is attributed to frequency instability of the gyrotron. Using these frequencies, the ^{13}C Larmor frequency, and the condition for the double-quantum solid effect condition, the frequency-agile gyrotron is then calibrated so that electron decoupling chirps effectively cover the N@C_{60} electron spin resonance.

For electron decoupling and off-resonance/control experiments, a period of DNP transfer from electron to the ^{13}C spins occurs between a ^{13}C-spin ''saturation train'' and a ^{13}C excitation pulse ($\pi/2$), which is followed by a rotor-synchronized refocusing pulse (Hahn echo, π). All ^{13}C pulses applied have a nutation frequency of 83 kHz (3 μs pulse = $\pi/2$). These experiments are performed at a magnetic field of 7.05 T (75.49 MHz

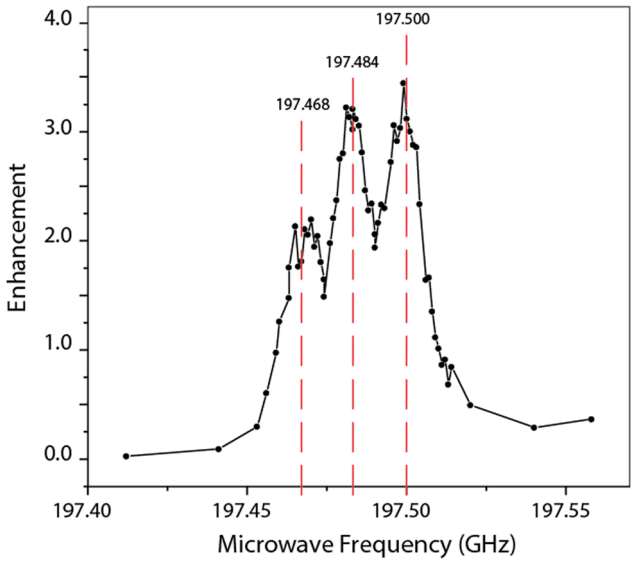

Fig. 3 DNP profile of N@C_{60} with 30 s DNP-transfer period. Each point represents the ^{13}C signal intensity of a 16-transient DNP experiment. The "enhancement" value is calculated as the difference in signal intensity between experiments with and without microwave irradiation, divided by the signal intensity from the experiment without microwave irradiation.

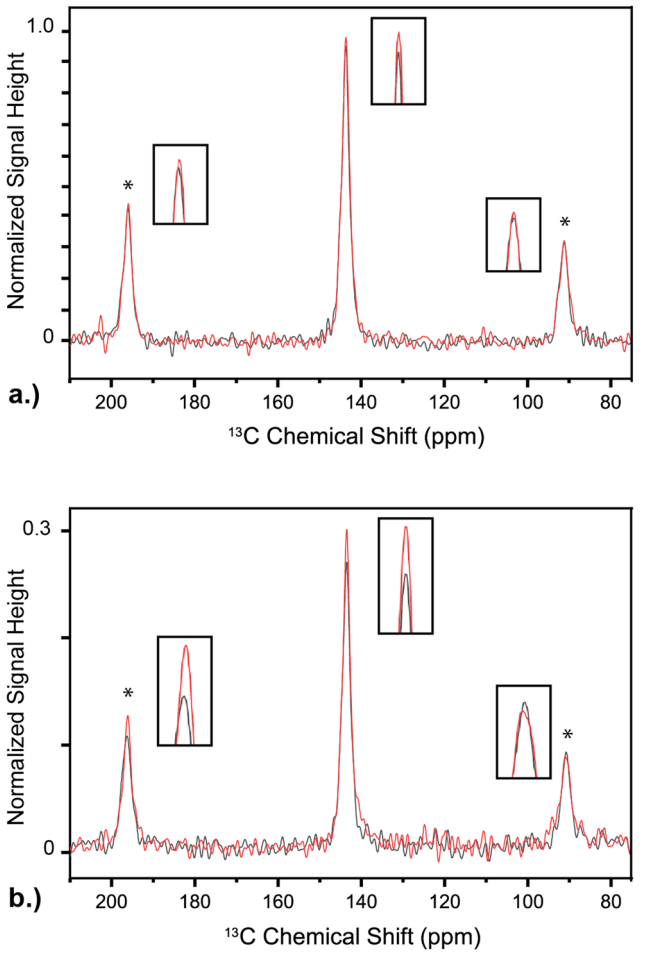

Fig. 4 (a) Comparison of signal obtained with (red) and without (black) electron decoupling following a 30 s DNP transfer. (b) Comparison of signal obtained with (red) and without (black) electron decoupling following a 7 s DNP period. The vertical scale is normalized to the height of the largest signal (30 s, isotropic peak). First-order spinning sidebands are feature an asterisk atop. Call-outs of peaks are featured adjacent to their corresponding signals to highlight changes in intensity.

^{13}C Larmor frequency) and at a temperature of 90 K, with a 3.2 mm cylindrical rotor spinning at 4.0 kHz (±5 Hz). A vacuum-jacketed cryogenic transfer/recovery system allows for stable MAS DNP operation at 90 K.[40,41] The frequency-agile gyrotron is controlled by a spectrometer-integrated arbitrary waveform generator (Tecmag Inc.). This, in series with a high voltage amplifier, alters the gyrotron anode potential, changing the microwave frequency.

Fig. 4a and b show the comparisons of electron-decoupled, DNP-enhanced NMR signal (red) to DNP-enhanced signal acquired without electron decoupling (black) for experiments with 30 s and 7 s DNP-transfer periods, respectively. The 30 s spectra are summations of 320 transients each, and the 7 s spectra are 2048 transients. After a 30 s DNP transfer, the only significant improvement is observed on the isotropic peak at 143.6 ppm.[42,43] Here, electron decoupling improves signal intensity by 5%. The effect of electron decoupling is greater for a 7 s DNP transfer, with a 12% improvement in signal intensity for the isotropic, central peak, and a 15% improvement for the spinning sideband at 196.6 ppm. The spinning sideband at 90.6 ppm shows no significant improvement in signal intensity with electron decoupling. All spectra are processed using tNMR software, and signal integration and linewidths are obtained using DMfit.[44]

The induced broadening from the electron-nuclear hyperfine interaction has been shown to completely attenuate ^{13}C NMR signal at high N@C_{60} concentrations (N@C_{60} : C_{60} at a 3 : 2 ratio).[45] Shorter DNP-transfer periods enhance nuclear spins that are closer to the polarizing electron spins, effectively increasing the ratio of paramagnetic endofullerenes to ^{13}C spins that contribute to observed, DNP-enhanced NMR signal. In this sample, the DNP build-up time is characterized by a time constant of 31 s, thus the difference in number of enhanced nuclear spins between 7 s and 30 s DNP transfer periods is noticeable (see relative vertical scales, signal-to-noise ratios in Fig. 4).[46] As the DNP-transfer period is increased, spin diffusion spreads the improved polarization to ^{13}C nuclei with weaker dipolar contact to the polarizing electron spins. The signal from these ^{13}C spins will not be improved by electron decoupling; this same effect is observed when electron decoupling trityl-based radicals.[1,6,7] Here a shorter DNP period results in greater electron decoupling effect, but the same trend is expected with higher concentration of N@C_{60}.

An interesting feature of the 7 s DNP experiments is the dissimilarity in the recovery of intensity between the first-order spinning sidebands upon electron decoupling (Fig. 4b). This difference suggests a change in asymmetry parameter associated with the chemical shift anisotropy (CSA) of the ^{13}C spins between the decoupled and non-decoupled spectra.[47,48] As this effect is not observed with electron decoupling following 30 s

DNP, a possible explanation is that the ^{13}C CSA of spins local or near to $N@C_{60}$ is non-identical to that of bulk ^{13}C (those not close to $N@C_{60}$). Similar to the efficacy of electron decoupling, this effect is also highlighted at shorter DNP periods, when $N@C_{60}$-proximal ^{13}C spins are enhanced to a greater extent than the bulk, $N@C_{60}$-distal spins.

Electron-decoupled MAS DNP using $N@C_{60}$ as a polarizing agent is a step toward utilizing the unique properties of $N@C_{60}$ for powerful experiments in MAS NMR/EPR. $N@C_{60}$ and other endofullerene species are the focus of innovations in quantum bit engineering and small molecule study, as well as novel DNP techniques and use of the electron spin as an environmental sensor.[49–58] Localized DNP with $N@C_{60}$ can be extended to more significant systems, such as the interior of a lipid bilayer membrane where surrounding proton spins from the lipid tails should afford an improved rate of polarization transfer, or to catalyst surfaces where a functionalized C_{60} cage may be exploited.[59,60] Combined with advances in endofullerene generation, frequency-agile gyrotrons can expand the application of MAS DNP using endofullerenes, and establish the practice of integrated NMR/EPR with MAS and at high magnetic field.

Conflicts of interest

There are no conflicts to declare.

Acknowledgements

We thank Dr Daniel Klose for his assistance with EPR experiments, and the reviewers for their insightful comments. Funding for this work is provided through the Swiss National Science Foundation (SNSF 201070).

Notes and references

1 E. P. Saliba, E. L. Sesti, F. J. Scott, B. J. Albert, E. J. Choi, N. Alaniva, C. Gao and A. B. Barnes, *J. Am. Chem. Soc.*, 2017, **139**, 6310–6313.
2 E. P. Saliba, E. L. Sesti, N. Alaniva and A. B. Barnes, *J. Phys. Chem. Lett.*, 2018, **9**, 5539–5547.
3 L. R. Becerra, G. J. Gerfen, R. J. Temkin, D. J. Singel and R. G. Griffin, *Phys. Rev. Lett.*, 1993, **71**, 3561–3564.
4 M. Afeworki, R. A. McKay and J. Schaefer, *Macromolecules*, 1992, **25**, 4084–4091.
5 B. Corzilius, *Phys. Chem. Chem. Phys.*, 2016, **18**, 27190–27204.
6 N. Alaniva, E. P. Saliba, E. L. Sesti, P. T. Judge and A. B. Barnes, *Angew. Chem.*, 2019, **58**, 7259–7262.
7 E. L. Sesti, E. P. Saliba, N. Alaniva and A. B. Barnes, *J. Magn. Reson.*, 2018, **295**, 1–5.
8 P. T. Judge, E. L. Sesti, L. E. Price, B. J. Albert, N. Alaniva, E. P. Saliba, T. Halbritter, S. T. Sigurdsson, G. B. Kyei and A. B. Barnes, *J. Phys. Chem. B*, 2020, **124**, 2323–2330.
9 T. J. Reddy, T. Iwama, H. J. Halpern and V. H. Rawal, *J. Org. Chem.*, 2002, **67**, 4635–4639.
10 P. T. Judge, E. L. Sesti, E. P. Saliba, N. Alaniva, T. Halbritter, S. T. Sigurdsson and A. B. Barnes, *J. Magn. Reson.*, 2019, **305**, 51–57.
11 T. A. Murphy, T. Pawlik, A. Weidinger, M. Höhne, R. Alcala and J.-M. Spaeth, *Phys. Rev. Lett.*, 1996, 1075–1078.
12 H. W. Kroto, J. R. Heath, S. C. O'Brien, R. F. Curl and R. E. Smalley, *Nature*, 1985, **318**, 162–163.
13 N. Weiden, H. Käss and K. P. Dinse, *J. Phys. Chem. B*, 1999, **103**, 9826–9830.
14 A. E. Douglas, *Nature*, 1977, **269**, 130–132.
15 J. J. Wittmann, T. V. Can, M. Eckardt, W. Harneit, R. G. Griffin and B. Corzilius, *J. Magn. Reson.*, 2018, **290**, 12–17.
16 K.-P. Dinse, H. Käß, C. Knapp and N. Weiden, *Carbon*, 2000, **38**, 1635–1640.
17 S. Knorr, A. Grupp, M. Mehring, M. Waiblinger and A. Weidinger, *AIP Conf. Proc.*, 2001, **544**, 191–194.
18 C. Knapp, N. Weiden and K. P. Dinse, *Magn. Reson. Chem.*, 2005, **43**, 199–204.
19 A. A. Smith, B. Corzilius, A. B. Barnes, T. Maly and R. G. Griffin, *J. Chem. Phys.*, 2012, **136**, 1–16.
20 G. Menzildjian, M. Y. A. Lund, D. Gajan, L. Niccoli, G. Karthikeyan, G. Casano, G. Jeschke, O. Ouari, M. Lelli and A. Lesage, *J. Phys. Chem. B*, 2021, **125**, 13329–13338.
21 A. C. Torrezan, S. T. Han, I. Mastovsky, M. A. Shapiro, J. R. Sirigiri, R. J. Temkin, A. B. Barnes and R. G. Griffin, *IEEE Trans. Plasma Sci.*, 2010, **38**, 1150–1159.
22 F. J. Scott, E. P. Saliba, B. J. Albert, N. Alaniva, E. L. Sesti, C. Gao, N. C. Golota, E. J. Choi, A. P. Jagtap, J. J. Wittmann, M. Eckardt, W. Harneit, B. Corzilius, S. T. Sigurdsson and A. B. Barnes, *J. Magn. Reson.*, 2018, **289**, 45–54.
23 A. Equbal, K. Tagami and S. Han, *J. Phys. Chem. Lett.*, 2019, **10**, 7781–7788.
24 C. Gao, N. Alaniva, E. P. Saliba, E. L. Sesti, P. T. Judge, F. J. Scott, T. Halbritter, S. T. Sigurdsson and A. B. Barnes, *J. Magn. Reson.*, 2019, **308**, 1–10.
25 D. E. Hoff, B. J. Albert, E. P. Saliba, F. J. Scott, E. J. Choi, M. Mardini and A. B. Barnes, *Solid State Nucl. Magn. Reson.*, 2015, **72**, 79–89.
26 T. V. Can, K. O. Tan, C. Yang, R. T. Weber and R. G. Griffin, *J. Magn. Reson.*, 2021, **329**, 1–7.
27 G. Mathies, S. Jain, M. Reese and R. G. Griffin, *J. Phys. Chem. Lett.*, 2016, **7**, 111–116.
28 S. K. Jain, G. Mathies and R. G. Griffin, *J. Chem. Phys.*, 2017, **147**, 1–13.
29 T. V. Can, R. T. Weber, J. J. Walish, T. M. Swager and R. G. Griffin, *Angew. Chem.*, 2017, **56**, 6744–6748.
30 P. Jakes, K. P. Dinse, C. Meyer, W. Harneit and A. Weidinger, *Phys. Chem. Chem. Phys.*, 2003, **5**, 4080–4083.
31 S. Abe, G. Sato, T. Kaneko, T. Hirata, R. Hatakeyama, K. Yokoo, S. Ono, K. Omote and Y. Kasama, *Jpn. J. Appl. Phys.*, 2006, **45**, 8340–8343.
32 A. Weidinger, M. Waiblinger, B. Pietzak and T. A. Murphy, *Appl. Phys. A*, 1998, **66**, 287–292.
33 H. Huang, M. Ata and M. Ramm, *Chem. Commun.*, 2002, 2076–2077.

34 T. Akasaka, N. Shigeru, B. Pietzak, A. Weidinger, K.-P. Dinse, A. Hirsch and Y. Kubozono, *Dev. Fullerene Sci.*, 2002, 13–65.
35 T. Kaneko, S. Abe, H. Ishida and R. Hatakeyama, *Phys. Plasmas*, 2007, **14**, 1–3.
36 S. C. Cho, T. Kaneko, H. Ishida and R. Hatakeyama, *Trans. Mat. Res. Soc. Japan*, 2012, **37**, 169–172.
37 S. C. Cho, T. Kaneko, H. Ishida and R. Hatakeyama, *J. Appl. Phys.*, 2015, **117**, 1–5.
38 K. Furukawa, S. Okubo, H. Kato, H. Shinohara and T. Kato, *J. Phys. Chem. A*, 2003, **107**, 10933–10937.
39 W. Harneit, K. Huebener, B. Naydenov, S. Schaefer and M. Scheloske, *Phys. Status Solidi B*, 2007, **244**, 3879–3884.
40 F. J. Scott, N. Alaniva, N. C. Golota, E. L. Sesti, E. P. Saliba, L. E. Price, B. J. Albert, P. Chen, R. D. O'Connor and A. B. Barnes, *J. Magn. Reson.*, 2018, **297**, 23–32.
41 B. J. Albert, S. H. Pahng, N. Alaniva, E. L. Sesti, P. W. Rand, E. P. Saliba, F. J. Scott, E. J. Choi and A. B. Barnes, *J. Magn. Reson.*, 2017, **283**, 71–78.
42 H. He, J. T. Dias, J. Foulkes and J. Klinowski, *Phys. Chem. Chem. Phys.*, 2000, **2**, 2651–2654.
43 R. Johnson, D. S. Bethune and C. S. Yannoni, *Acc. Chem. Res.*, 1992, **25**, 169–175.
44 D. Massiot, F. Fayon, M. Capron, I. King, S. L. Calvé, B. Alonso, J. O. Durand, B. Bujoli, Z. Gan and G. Hoatson, *Magn. Reson. Chem.*, 2002, **40**, 70–76.
45 H. Nikawa, Y. Araki, Z. Slanina, T. Tsuchiya, T. Akasaka, T. Wada, O. Ito, K. P. Dinse, M. Ata, T. Kato and S. Nagase, *Chem. Commun.*, 2010, **46**, 631–633.
46 J. J. Wittmann, M. Eckardt, W. Harneit and B. Corzilius, *Phys. Chem. Chem. Phys.*, 2018, **20**, 11418–11429.
47 R. Tycko, R. C. Haddon, G. Dabbagh, S. H. Glarum, D. C. Douglass and A. M. Mujsce, *J. Phys. Chem.*, 1991, **95**, 518–520.
48 W. I. F. David, R. M. Ibberson, T. J. S. Dennis, J. P. Hare and K. Prassides, *Europhys. Lett.*, 1992, **18**, 219–225.
49 W. Harneit, *Endohedral Fullerenes: Electron Transfer and Spin*, 2017, pp. 297–324.
50 J. E. Grose, E. S. Tam, C. Timm, M. Scheloske, B. Ulgut, J. J. Parks, H. D. Abruña, W. Harneit and D. C. Ralph, *Nat. Mater.*, 2008, **7**, 884–889.
51 N. Roch, R. Vincent, F. Elste, W. Harneit, W. Wernsdorfer, C. Timm and F. Balestro, *Phys. Rev. B: Condens. Matter Mater. Phys.*, 2011, **83**, 1–4.
52 W. Harneit, C. Boehme, S. Schaefer, K. Huebener, K. Fostiropoulos and K. Lips, *Phys. Rev. Lett.*, 2007, **98**, 1–4.
53 S. Schaefer, K. Huebener, W. Harneit, C. Boehme, K. Fostiropoulos, H. Angermann, J. Rappich, J. Behrends and K. Lips, *Solid State Sci.*, 2008, **10**, 1314–1321.
54 S. Zhou, M. Yamamoto, G. A. D. Briggs, H. Imahori and K. Porfyrakis, *J. Am. Chem. Soc.*, 2016, **138**, 1313–1319.
55 J. J. Morton, A. M. Tyryshkin, A. Ardavan, S. C. Benjamin, K. Porfyrakis, S. A. Lyon and G. A. D. Briggs, *Nat. Phys.*, 2006, **243**, 3028–3031.
56 J. J. Morton, A. M. Tyryshkin, A. Ardavan, K. Porfyrakis, S. A. Lyon and G. A. D. Briggs, *Phys. Rev. B: Condens. Matter Mater. Phys.*, 2007, **76**, 1–6.
57 B. Meier, S. Mamone, M. Concistrè, J. Alonso-Valdesueiro, A. Krachmalnicoff, R. J. Whitby and M. H. Levitt, *Nat. Commun.*, 2015, **6**, 1–4.
58 D. Pinto, D. Paone, B. Kern, T. Dierker, R. Wieczorek, A. Singha, D. Dasari, A. Finkler, W. Harneit, J. Wrachtrup and K. Kern, *Nat. Commun.*, 2020, **11**, 1–6.
59 K. A. Russ, P. Elvati, T. L. Parsonage, A. Dews, J. A. Jarvis, M. Ray, B. Schneider, P. J. Smith, P. T. Williamson, A. Violi and M. A. Philbert, *Nanoscale*, 2016, **8**, 4134–4144.
60 R. S. D'Rozario, C. L. Wee, E. J. Wallace and M. S. Sansom, *Nanotechnology*, 2009, **20**, 1–7.